Journal of Thermal Analysis and Calorimetry, Vol. 59 (2000) 451–470

Dedicated to Prof. Edith A. Turi in recognition of her leadership in education

APPLICATIONS OF SUCCESSIVE SELF-NUCLEATION AND ANNEALING (SSA) TO POLYMER CHARACTERIZATION

M. L. Arnal[1], *V. Balsamo*[1], *G. Ronca*[1], *A. Sánchez*[2], *A. J. Müller*[1*], *E. Cañizales*[3] *and C. Urbina de Navarro*[3]

[1]Grupo de Polímeros USB, Departamento de Ciencia de los Materiales, Universidad Simón Bolívar, Apartado 89000, Caracas 1080-A
[2]Departamento de Mecánica, Universidad Simón Bolívar, Apartado 89000, Caracas 1080-A
[3]Centro de Microscopía Electrónica, Facultad de Ciencias, Universidad Central de Venezuela Caracas, Venezuela

Abstract

A new technique to thermally fractionate polymers using DSC has been recently developed in our laboratory. The applications of the novel successive self-nucleation and annealing (SSA) technique to characterize polyolefins with very dissimilar molecular structures are presented as well as the optimum conditions to thermally fractionate any suitable polymer sample with SSA. For ethylene/α-olefin copolymers, the SSA technique can give information on the distribution of short chain branching and lamellar thickness. In the case of functionalized polyolefins, detailed examinations of SSA results can help to establish possible insertion sites of grafted molecules. The application of the technique to characterize crosslinked polyethylene and crystallizable blocks within ABC triblock copolymers is also presented.

Keywords: annealing, DSC, self-nucleation, SSA, thermal fractionation

Introduction

The technique of successive self-nucleation and annealing (SSA) has been recently developed in our laboratory to characterise semicrystalline polymers that are capable of undergoing molecular segregation during crystallization upon cooling from the melt using DSC [1–5].

SSA is essentially a thermal fractionation method that is based on the sequential application of self-nucleation and annealing steps to a polymer sample. After thermal conditioning a final DSC heating run reveals the distribution of melting points induced by the SSA treatment as a result of the heterogeneous nature of the chain structure of the polymer under analysis. The nature of the polymer chain must be heterogeneous in order to have a wide distribution of crystallizable chain segments, such as in random ethylene/α-olefin copolymers, cross-linked polyethylenes or confined chains of crystallizable polymers within microphase separated block copolymers.

* Author for correspondence: e-mail: amuller@usb.ve

1418–2874/2000/ $ 5.00

Akadémiai Kiadó, Budapest
Kluwer Academic Publishers, Dordrecht

The versatility in physical properties of ethylene/α-olefin copolymers depends on the type, amount and distribution of the α-olefin comonomer. The influence of the distribution of the α-olefin along the chain is particularly important [6–9], a fact intimately connected to the nature and type of the catalytic system employed during the ethylene copolymerization [9–10]. Many of these copolymers can exhibit a highly heterogeneous comonomer distribution in the sense that the distribution of the short chain branches (SCB) is heterogeneous along one particular chain, and each chain or group of chains may possess a different chain branching distribution [10–13].

The particular interest to characterize the comonomer distribution in linear low density polyethylenes (LLDPE, ethylene/α-olefin copolymers) led to the development of temperature rising elution fractionation (TREF). This technique produces separation by the elution of polymer fractions at successively rising temperatures of a material that has been allowed to crystallize from solution on an inert support during very slow cooling or multiple steps. Such slow crystallization from solution favors molecular segregation by short chain branching content and distribution with a limited influence of molecular mass [11]. Even though the technique has been successfully applied, its implementation can be difficult and expensive and measurement times can be long.

If a rapid characterization of an ethylene/α-olefin copolymer is desired, then TREF might not be a practical option. This is why several authors have develop quicker and easier thermal fractionation methods using DSC: such methods involve step-crystallization (SC) from the melt, a technique that is based on the step crystallization from solution that is applied in the TREF technique. These SC methods can provide qualitative preliminary information on the comonomer distributions of the polymer under study in less time and without any additional instrumentation than a conventional DSC [10, 14–23].

We have shown in previous works that SSA produces better fractionation than SC [1–2] using shorter times since the method involves a more complex thermal treatment that allows better resolution. The SSA method is based on a superposition of self-nucleation and annealing cycles, where each cycle is similar to those designed by Fillon *et al*. [24] for the evaluation of the self-nucleation process in polypropylene (PP), a procedure used by our group in the past to study the fractionated crystallization of polyolefins dispersed in immiscible matrices [25–28].

In this work, we have chosen one ethylene/α-olefin copolymer (a linear low density polyethylene, LLDPE) to demonstrate the usefulness of SSA as a thermal fractionation technique and its application to calculate approximate short chain branching (SCB) and lamellar thickness distributions. The application of SSA to characterize different types of polymers is also presented here, the polymers studied include: functionalized ultra low density polyethylene (ULDPE), a crosslinked low density polyethylene (XLDPE) used for high voltage wire insulation and crystallizable blocks within ABC triblock copolymers.

Experimental

Materials

The neat polymers used in this study were: a blown film grade LLDPE-b 11U4 ethylene/1-butene copolymer synthesized by a solution process by Resilin (Venezuela), previously characterized via TREF [13]; an ultra low-density polyethylene (ULDPE) Nuld2 ethylene/propene/1-butene copolymer of Enichem Polimeri (Italy), produced in a modified high pressure process using supported Ziegler-Natta (Z-N) catalysis; LDPE HFDA 4201 NT EC from Union Carbide with crosslinking agent.

Three polystyrene-*block*-poly(ethylene-co-butylene)-*block*-poly(ε-caprolactone) triblock copolymers (SEC) prepared by in a previous work [29] will be used here: $S_{27}E_{37}C_{36}^{132}$, $S_{27}E_{15}C_{58}^{219}$, $S_{57}E_{27}C_{16}^{137}$. This abbreviated nomenclature includes the mass percentage of each component as subindices and the number average molecular masses of the triblock copolymers as superindices. Their molecular characteristics can be found in [29].

Some physical characteristics of the polymers used are presented in Table 1. Four solution grafted maleic anhydride ULDPE were obtained by employing different maleic anhydride (MAH) and initiator concentrations according to the procedure described elsewhere [2, 30]. The grafting reaction conditions are presented in Table 2.

DSC

The neat polymers were compression molded into 0.5 mm sheets; from these sheets small disc samples were cut (10 mg). The samples were encapsulated in aluminum pans and high purity dry nitrogen was used as an inert atmosphere for all tests in a Perkin Elmer DSC7 or PYRIS-1. For a previous characterization of thermal behavior of neat polymers, DSC cooling and heating curves were performed at 10°C min^{-1} after the samples were held in the melt (see below) for 3 min in order to erase all previous thermal history. More complex thermal treatments like SSA were employed and are described below.

Self-nucleation experiments (SN)

Since SSA is based on the accumulation of self-nucleation and annealing steps, we will first describe how to perform single self-nucleation and annealing experiments using DSC as it was originally conceived by Fillon *et al*. [24]. These experiments involved the partial melting of a crystalline 'standard' state followed by recrystallization using as nuclei the crystal fragments produced in the partial melting stage. The detailed procedure is described as follows:

a) Erasure of previous thermal history: the sample was kept at a melting temperature for 3 min. The initial melting temperature is chosen to be much higher than the peak melting temperature (T_m) of the polymer under study in order to erase any previous thermal history, typically a temperature of at least 25°C higher than T_m is chosen.

Table 1 Basic characteristics of the materials used in this study

Materials	MFI/dg min^{-1}	Density/g cm^{-3}	$\overline{M}_w$ and polydispersity	SCB content[1] [–CH_3/1000°C]	T_c/°C	T_m/°C	X_c[2]/%
ULDPE Nuld2	1.3	0.875	–	88.0	86	107	19
LLDPE-b 11 U4	1.4	0.922	159, 700/4.2	12.7	102	119	43
LDPE HFDA-4201 NTEC[3]	–	0.920	58, 800	–	–	106	33
XLDPE[4]	–	0.910	–	–	–	101.4	28

[1]Short chain branching.
[2]Peak crystallization and melt temperature (T_c, T_m) at 10°C min^{-1} and crystallinity (X_c) calculated by DSC heating scans at the same heating rate.
[3]This polymer was purified to extract the crosslinking agent.
[4]The HFDA-4201 NT EC was crosslinked with 2% dicumil peroxide under nitrogen atmosphere at 204°C.

Table 2 Grafting reaction conditions for ULDPE

Materials	MAH/pph	*I*/pph	Grafting degree[1]/ g MAH/100 g PE	T_m/°C	X_c/%
ULDPE-G4	5	0.3	0.20	103.4	18.1
ULDPE-G8	10	0.3	0.54	103.2	18.9
ULDPE-G12	5	1.5	0.72	98.7	17.4
ULDPE-G16	10	1.5	1.51	98.0	15.8

[1]Determined by an FTIR-titration calibration curve.

This initial melting at this maximum temperature leaves only temperature-resistant heterogeneous nuclei of unknown nature.

b) Creation of the initial 'standard' state: the sample was cooled at a rate of 10°C min^{-1} down to a minimum temperature that should be low enough to allow sample crystallization during the controlled cooling. Then, the sample is held for 10 min at that minimum temperature. For the polyolefins used here this minimum temperature was 25°C. In the block copolymers case, this temperature was 50°C.

c) Self-nucleation: the sample was heated at 10°C min^{-1} from the chosen minimum temperature up to a selected self-seeding temperature (that we shall termed T_s) located in the final melting temperature range of the sample, and it was held at that temperature for 5 min. This isothermal treatment at T_s results in partial melting and, depending on T_s, in the annealing of unmelted crystals, while some of the melted species may isothermally crystallize (after being self-nucleated by the unmelted crystals).

d) Final crystallization: subsequent cooling at 10°C min^{-1} from T_s down to the chosen minimum temperature. During this cooling the initially molten fraction of the polymer at T_s will crystallize during cooling using the unmelted crystal fragments produced by partial melting in step 'c' as self-nuclei.

e) Final melting: subsequent heating at 10°C min^{-1} from the chosen minimum temperature up to the maximum melting temperature established in step 'a'.

SSA experiments

The SSA technique enhances the potential molecular fractionation that can occur during crystallization, while encouraging annealing of the unmelted crystals at each stage of the process, so that small effects can be magnified.

Experimentally, the steps 'a' to 'c' of the SN method described above were repeated as the first part of this experiment. Special care should be taken to choose the first T_s temperature to be used in step 'c'.

Ideally the first T_s should be high enough to melt most of the polymer, but low enough to leave some crystal fragments that can act as nuclei but will not anneal during the 5 min at that T_s (the importance of the value of the first T_s temperature used will be discussed below).

The following steps were performed immediately after steps 'a' to 'c':

d) Cooling from T_s: The sample was cooled at 10°C min^{-1} from T_s down to the chosen minimum temperature. During this cooling the initially molten fraction of the polymer at T_s will crystallize during cooling using the unmelted crystal fragments produced in step 'c' as self-nuclei.

e) Heating to a new T_s: The sample was heated once again at 10°C min^{-1}, but this time up to a T_s temperature which was 5°C lower than the previous T_s and held at that temperature for 5 min. This means that the unmelted crystals at this T_s will anneal, some of the melted species may isothermally crystallize (after being self-nucleated by the unmelted crystals) while the rest of the molten crystallizable chain segments will only crystallize during the subsequent cooling from T_s.

f) Steps 'd' and 'e' are repeated at increasingly lower T_s: The differences in T_s were always kept constant at 5°C. The number of repetitions can be chosen to cover the entire melting range of the sample with a 'standard' thermal history or a shorter range.

g) Final melting: The sample was heated at 10°C min^{-1} from the chosen minimum temperature up to the maximum melting temperature established in step 'a'.

Figure 1 shows a schematic diagram that illustrates the thermal cycles applied during the SSA technique to LLDPE. Table 3 lists the SSA conditions applied to each polymer sample.

Table 3 Conditions used for the SSA treatments

Materials	T_{max}[1]/°C	T_{min}[2]/°C	T_s range[3]/°C
LLDPE-b 11 U4	170	30	123–58
ULDPE $N_{ULD}2$	170	30	124–59
ULDPE-G4	170	30	124–59
ULDPE-G8	170	30	124–59
ULDPE-G12	170	30	124–59
ULDPE-G16	170	30	124–59
LDPE HFDA-4201 NTEC[3]	160	25	105–50
XLDPE	160	25	105–50
$S_{27}E_{37}C_{36}^{132}$	140	50	90–60
$S_{57}E_{27}C_{16}^{137}$	140	50	90–65
$S_{27}E_{15}C_{58}^{219}$	140	50	90–65

[1]Initial maximum melting temperature. [2]Minimum temperature used in SSA thermal cycles.
[3]Range of T_s temperatures employed separated by 5°C intervals.

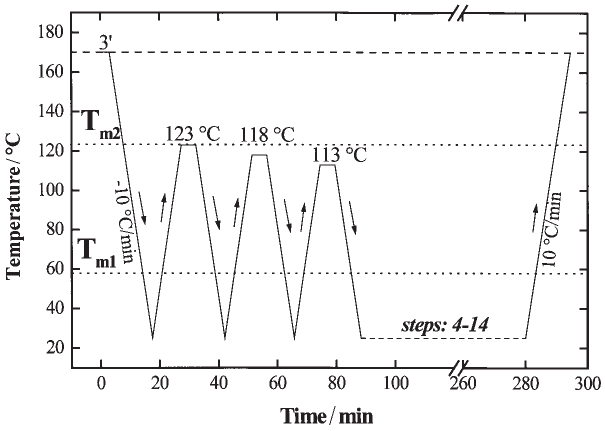

Fig. 1 Schematic representation of successive self-nucleation/annealing (SSA) thermal treatment (e.g., as applied to LLDPE), where T_{m1} and T_{m2} define the T_s range applied (Table 3 and text). The T_s temperatures in this case were varied from 123 to 58°C at 5°C intervals for a total of 14 self-nucleating/annealing steps

Transmission electron microscopy

Before TEM observation a LLDPE sample was prepared by 75 min etching in permanganic acid followed by replication according to the method developed by Olley *et al*. [31].

Results and discussion

Characterization of LLDPE by SN and SSA

Figures 2 and 3 present the self-nucleation behavior of the LLDPE. Figure 2 shows the cooling runs after thermal conditioning at the indicated T_s and Fig. 3 shows the subsequent heating runs. Table 4 lists all the relevant transition temperatures for the LLDPE taken from Figs 2 and 3.

The heterogeneous nature of the short chain branching (SCB) distribution of this LLDPE is evidenced in the broad crystallization range that extends from 110°C down to 35°C, this behavior is characteristic of ethylene/α-olefin copolymers that have been prepared by Ziegler-Natta type catalysts [10, 13]. Furthermore, a previous temperature rising elution fractionation (TREF) study [13] on this LLDPE has demonstrated that this polymer has a bimodal distribution of SCB. This is also reflected on the cooling DSC trace of Fig. 2 (at T_s=170°C), where one relatively sharp crystallization exotherm is followed by a wide tail. The first peak corresponds to the crystallization of the linear portions of the less branched chains that usually crystallize at higher temperatures, the low temperature tail corresponds to the crystallization of the shorter linear portions of chains with higher content of SCB. The heterogeneous SCB distribution of this LLDPE produces upon cooling the formation of a bimodal distribution of lamellar thickness that later in the subsequent heating run, melt with a broad bi-

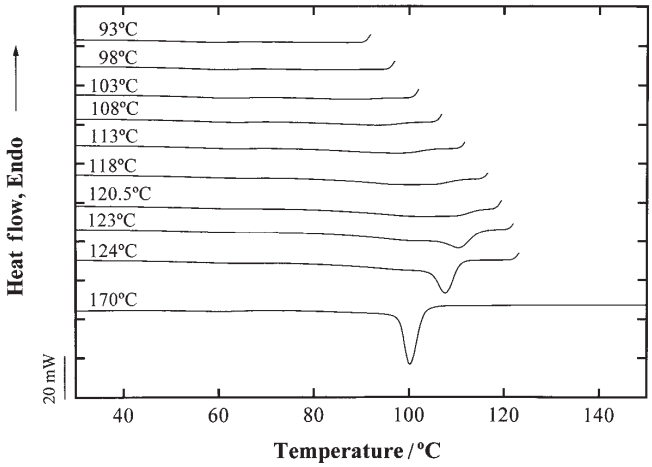

Fig. 2 DSC cooling curves after self-nucleation at the indicated T_s temperatures for LLDPE

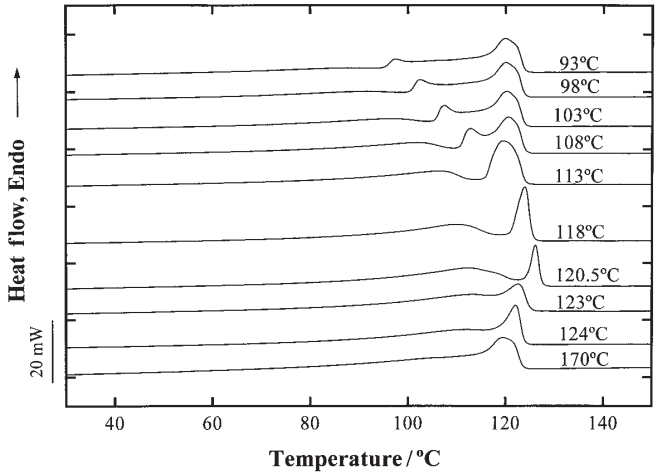

Fig. 3 DSC heating curves for LLDPE after the cooling shown in Fig. 2

modal distribution of melting points (Fig. 3, melting curve after cooling from 170°C or later, Fig. 5).

Table 4 Thermal characterization of LLDPE

T_s/°C	T_c peak/°C	T_m peak/°C		
		A	B	C
170	100.1	119.5	*	
124	107.6	122.03	*	
123	110.3	122.5	*	
120.5	103.0	***126.2***	112.4	
118	99.6	***124.0***	110.0	
113	97.5	***119.5***	106.5	
108	93.5	120.7	***112.9***	102.0
103	88.3	120.2	***107.4***	*
98	93.5	120.0	***102.5***	*
93	89.0	120.0	***97.4***	*

*Not well defined melting peak.

Figure 4 shows a TEM micrograph of a sample of LLDPE that was cooled at 5°C min^{-1}. The lamellar morphology has been revealed by the etching of the amorphous part of the sample. An approximately bimodal distribution of lamellar thickness is apparent since thicker lamellae are very distinct from thinner ones. A wide range of lamellar thickness was obtained by direct measurements on Fig. 4 and by TEM observations made with other techniques [32]. The lamellar sizes obtained ranged from approximately 25 to 50 nm.

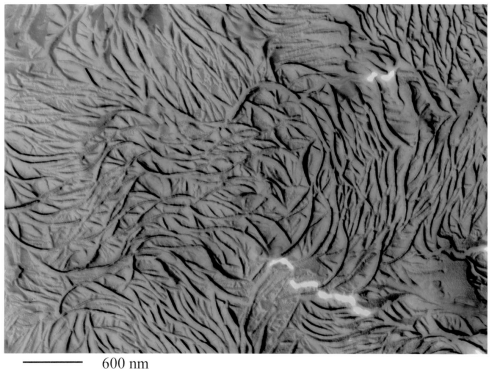

Fig. 4 TEM micrograph for LLDPE cooled from the melt at 5°C min^{-1}

Figure 2 shows the DSC cooling scans from a very wide range of T_s values. Fillon *et al*. [24] have defined the so-called domains of self-nucleation for PP and we shall use their nomenclature here. The polymer is said to be under domain I when complete melting occurs, in this case complete melting was found to persist down to 125°C, since no change was detected in the crystallization temperature as compared to the sample with a T_s temperature of 170°C, indicating that all crystalline memory has been erased.

At 124°C the LLDPE was self-nucleated by remanent crystal fragments and its crystallization temperature was shifted to higher temperatures while the subsequent melting did not reveal any traces of annealing, a characteristic behavior of domain II (i.e., only self-nucleation). The typical behavior of domain II was only detected in the narrow range of T_s temperatures comprising 124–123°C, while temperatures below or equal to 122°C produced self-nucleation and annealing, i.e. samples in domain III. Figure 2 shows as an example, that at a T_s of 120.5°C, the crystallization exotherm shows a characteristic shoulder [24] that indicates immediate crystallization upon cooling from T_s and the subsequent melting endotherm in Fig. 3 shows a high temperature sharp peak that is due to annealing at that T_s.

The characteristic behavior of the self-nucleation of the LLDPE presented in Figs 2 and 3 indicate as discussed above that the maximum temperature that induces self-nucleation without any annealing, or the minimum temperature of domain II is 123°C. We shall define this temperature as the optimum self-nucleation temperature or optimum T_s for this particular LLDPE. The location of the domains is qualitatively similar in this case to those reported for PP by Fillon *et al*. [24].

When the T_s temperature is lower than 113°C, three melting peaks can be observed in Fig. 3 (for the curve with T_s=108°C). This is a consequence of the lowering of the melting point of the annealed crystals as T_s is lowered. This can be seen also in Table 4. According to Table 4, for T_s=120.5°C self-nucleation and annealing occurred, where the T_m of the annealed crystals is reported to be 126.2°C (or peak labeled A in Table 4). As T_s is lowered, the melting point of the annealed crystals is progressively lowered, being 124°C for a T_s of 118°C (Fig. 3). Then at T_s=113°C, the melting point of the annealed crystals coincides with 119.5°C, which just happens to

be the melting point of the usual high temperature melting point of LLDPE (that of T_s=170°C in Table 4, which has been labeled peak A). At a T_s=108°C, the temperature is not high enough to affect the crystals that usually melt at around 119.5°C (i.e., peak A in Table 4), therefore the annealed crystals now melt at 112.9°C (i.e., peak B in Table 4). The lowest melting point for this sample with T_s=108°C, is that corresponding to the crystals formed during cooling from T_s or the peak labeled C in Table 4. A similar situation dominates the behavior for the DSC traces corresponding to T_s temperatures lower or equal to 108°C. In order to make this point clear, we have represented in bold and italics those melting points that correspond to the melting of annealed crystals at T_s in Table 4.

As a summary of the melting behavior displayed in Fig. 3 and Table 4 for the neat LLDPE, it should be noted that the LLDPE may possess up to a maximum of three melting peaks when annealing at T_s was present, since one peak corresponds to the melting of the annealed crystals and the other two peaks reflect whatever is left of the endothermic melting of the original bimodal population of lamellar thickness.

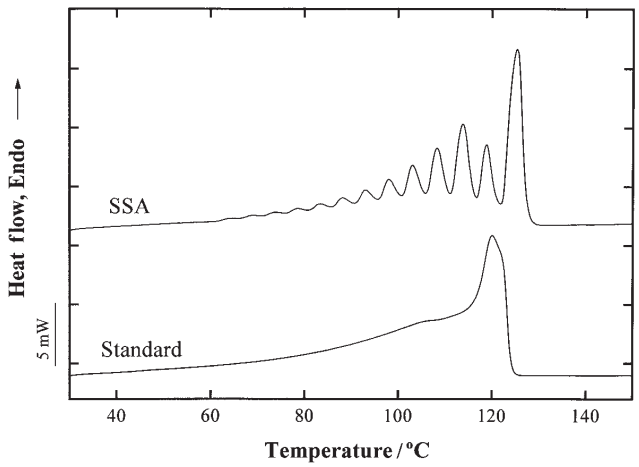

Fig. 5 DSC heating scans at 10°C min^{-1} for LLDPE. Bottom: after a controlled cooling at 10°C min^{-1}, and T_{op}: after SSA thermal treatment

Figure 5 shows heating DSC scans of neat LLDPE and of LLDPE after the SSA treatment (i.e., the final heating run of the SSA or step 'g' in the experimental part). The SSA curve shows the effects of the accumulation of 14 self-nucleation and annealing steps using T_s temperatures from 123 to 58°C every 5°C. Since 123°C does not cause any annealing because it is a T_s temperature within domain II, only 13 steps were able to produce annealing. The melting trace of LLDPE after SSA clearly shows 13 melting peaks in Fig. 5 illustrating the capability of the technique to induce thermal fractionation in view of the broad SCB distribution of the neat copolymer. The distribution of melting peaks shows a clear bimodal distribution that reflects the bimodal distribution of the SCB in the polymer [13].

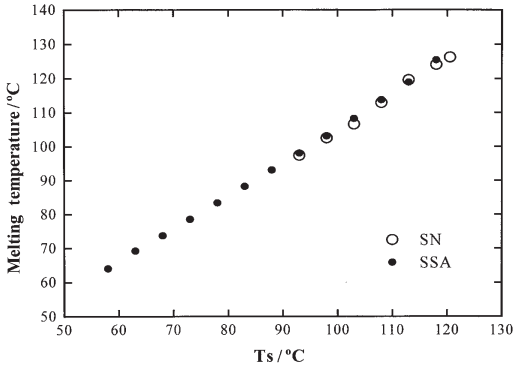

Fig. 6 Linear relationship between LLDPE melting points and selected T_s temperatures for annealed crystals. Open circles: single self-nucleation and annealing data points (i.e., values in bold and italics in Table 4). Filled circles: Successive self-nucleation and annealing data points (taken from the 12 peak melting temperatures of the DSC heating trace after SSA treatment shown in Fig. 5)

A very interesting comparison can be made on the results of the SSA and those of the self-nucleation process presented in Fig. 3. If a plot is made of T_s *vs*. melting peak for the 13 peaks of the final SSA melting trace, a very good straight line is generated that could for instance predict the melting point of the annealed crystals at a particular T_s within 1°C (Fig. 6). The melting points of the annealed crystals after self-nucleation from 118 until 93°C in Fig. 3 fit very well this tendency illustrating the fact that as stated above the SSA technique is a simple accumulation of individual self-nucleation and annealing steps. Figure 6 shows the melting points *vs*. T_s temperatures of both the individual annealing treatments shown in Fig. 3 (and in bold and italic font in Table 4) and those after the SSA treatment (Fig. 5 and Table 4). It can be observed in Fig. 6 that all the data points fall under a common straight line that has a correlation coefficient of 0.999.

Optimum conditions for SSA analysis

The SSA results presented in Fig. 5 were produced using optimum parameters for the fractionation. The most important parameters are: the first T_s temperature to be used, the temperature interval between T_s temperatures, the permanence time at T_s and the heating rates used during the thermal conditioning steps.

We strongly recommend to use in step 'c' of the SSA thermal conditioning the optimum self-nucleation temperature or optimum T_s temperature defined above (see Experimental), in this way the polymer would always be in the same starting condition (i.e., at the minimum temperature within domain II).

In a previous publication the influence of the time for each isothermal step, and the temperature intervals between the T_s temperatures to be used were studied using the same LLDPE employed in this work [2], including initially different scanning rates (5, 10 and 20°C min^{-1}). The resolution of the final heating scan was much better

for 5 and 10°C min^{-1} than for 20°C min^{-1}. It was observed that both 5 and 10°C min^{-1} produced similar results; a scanning rate of 10°C min^{-1} was then selected, because of the possibility to reduce testing time. Secondly, three different temperature intervals between each T_s were employed: 1, 2.5 and 5°C. Better fractionation was obtained for 2.5°C spacing between each T_s, because the number of endothermic signals obtained, at a given temperature interval, significantly increased as compared to 1 and 5°C temperature intervals. In fact, this increment in the number of signals after SSA, indicates a better segregation and fractionation due to the self-nucleation, isothermal crystallization and annealing effects promoted at this specific condition. For 1°C spacing, there was an overlapping of the signals, product of the overcoming of the resolution limit of the DSC equipment.

Finally, two holding times at the selected T_s temperatures were tested: five and fifteen min. The increase in holding time does not promote a higher number of signals. Nevertheless, more perfect crystals are formed and annealed in each step because the peak temperatures are about 1°C higher for 15 min holding time than for 5 min holding time. Because of the high time consumption with 15 min holding time, a 5 min holding time was selected for successful tests as well as 5°C spacing between each T_s (2.5°C spacing between each T_s can be used if a greater number of fractions is desired but the testing time will also increase). The short time span at T_s is one of the major advantages of the SSA technique as compared to SC, since in the latter much longer isothermal steps are needed in order to fractionate the samples.

The technique could also in principle fractionate linear chains of different molecular lengths, but in this case the times at each T_s have to be extremely long rendering the technique impractical, at least in the polyolefins case. The parameters given above have been designed to fractionate chains where the crystallizable sequences are separated by branches, or other irregularities (such as grafted functional groups, crosslinks, etc.). The effect of molecular mass distribution on the fractionation is therefore limited. If SSA is performed on a perfectly linear HDPE with a polydispersity of 10, almost no fractionation is obtained (the final heating scan only shows one single melting peak which may contain a shoulder depending on the specific sample used).

Determination of mean lamellar thickness distributions and of SCB distributions by SSA

The final heating run after an SSA treatment exhibits a series of melting peaks that correspond to the number of SSA cycles where annealing was promoted. The differential area under such fusion curve can be related to the number of lamellae that melt within the temperature interval considered. Thompson-Gibbs equation [33] can then be used to establish a correlation between temperature and lamellar thickness:

$$l=2\sigma T_m^0/\Delta H_v(T_m^0-T_m)$$

We have used the above equation choosing the same values reported by Stark [10] for the following parameters that were assumed to be constant: lamellar surface

free energy (σ: $70 \cdot 10^{-3}$ J m^{-2}), enthalpy of fusion for infinitely thick lamellae (ΔH: $288 \cdot 10^{6}$ J m^{-3}) and equilibrium melting temperature (T_m^0: 414.5 K). Lu *et al*. [34] have questioned the use of Thompson-Gibbs equation for the calculation of lamellar thickness distributions in ethylene/α-olefin copolymers, since it tends to underestimate the width of such distributions. The reason behind such problem according to these authors is the change in melt composition as fusion progresses, a fact that would indicate that neither σ nor ΔH is constant with temperature. Therefore, the values of mean lamellar thickness obtained in this work from the Thompson-Gibbs equation after the SSA treatment will only give a qualitative indication of the mean lamellar thickness distribution that can be useful for comparison purposes, specially since they can be quickly obtained via DSC. Rigorous determination of the lamellar thickness distribution can only be obtained by TEM or by Raman spectroscopy [34].

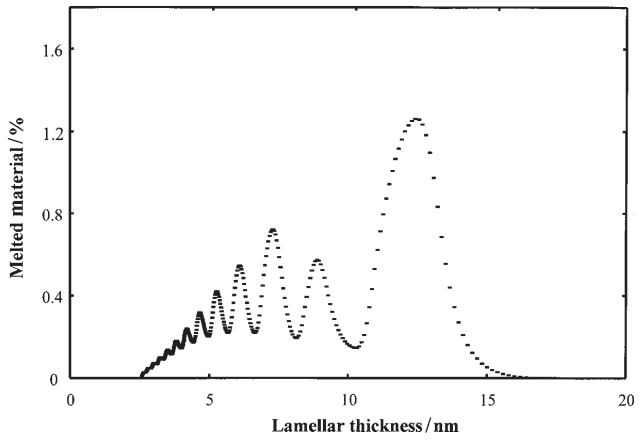

Fig. 7 Derived lamellar thickness distribution for LLDPE using SSA and the Thompson-Gibbs equation

If the SSA final melting run of Fig. 5 is integrated, a trace that is indicative of the proportion of material being melted (in %) as a function of temperature can be obtained [5]. This information is then used to calculate from the Thompson-Gibbs equation the distribution of lamellar thickness presented in Fig. 7. The distribution obtained is qualitatively similar to the SSA thermal fractionation curve of Fig. 5, but the width of the peaks had been modified. In particular, it can be noticed that the peaks corresponding to thicker lamellae are broader than those of thinner lamellae. This is a consequence of the mathematical simplicity of Thompson-Gibbs equation in predicting small lamellar thickness changes with major temperature changes at low apparent melting temperatures and big changes in lamellar thickness with small temperature changes at high apparent melting temperatures (i.e. closer to the T_m^0). These results agree with Mandelkern and Alamo observations regarding the limitations of the Thompson-Gibbs equation [34].

In spite of the limitations of the Thompson-Gibbs equation, a qualitative idea of the lamellar thickness distribution in the LLDPE sample used here was obtained by SSA. The obtained distribution shown in Fig. 7 can be compared with experimentally determined distributions by TEM. Even though a quantitative agreement was not expected since the thermal history is not the same, both distributions present approximate bimodal shapes with a relatively high frequency of thicker lamellae [32].

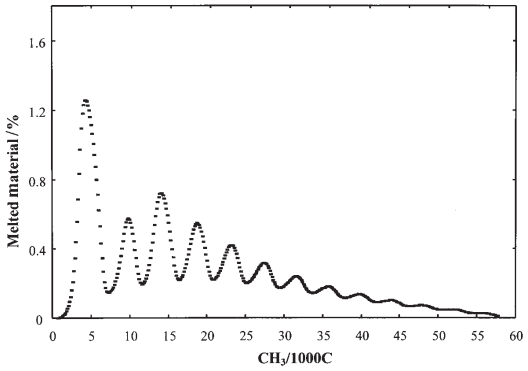

Fig. 8 Estimated short chain branching distribution for LLDPE based on TREF and SSA results

The apparent melting temperatures can also be related to the content of short chain branching (SCB) or comonomer distribution in ethylene/α-olefin copolymers when the type of comonomer is known and the relationship between T_m and the content of SCB has been determined by TREF. Since we had previously fractionated the LLDPE used here by TREF, we were able to obtain an equation to correlate T_m and SCB using the data of [13]. The melting point *vs*. SCB content of the fractions obtained for our LLDPE are correlated by the following equation:

$$T_m(°C)=130.2–1.2CH_3/1000°C$$

Figure 8 shows the distribution of SCB obtained after applying the above correlation to the thermally fractionated LLDPE of Fig. 5. Since the temperature axis was only linearly transformed, the shape of the distribution is identical to that of the SSA curve of Fig. 5 (except that it has been plotted in increasing branching order which corresponds to decreasing melting temperature). Therefore, if the SSA treatment is applied to an unknown LLDPE, at least a qualitative idea of its SCB distribution can be obtained (if the type of comonomer and synthesis method is known, some empirical correlations are available in the literature [10]) with a relatively quick DSC analysis.

Application of SSA to characterize ULDPE and ULDPE-g-MAH

Grafting of polar groups into polymers is an important method for the preparation of polyolefins with functional groups. It is of interest because these 'new materials' can be used to improve compatibility between the components of immiscible polymer

blends [35]. Solution functionalization reactions are well known [4, 36–37]. However, there is not a feasible technique for rapid characterization of molecular changes introduced by the grafting reaction. Application of the SSA method to functionalized polyolefins provides very useful information about probable location of functional groups on the polymer backbone [4]. In this work, maleic anhydride grafted ultra low density polyethylene (ULDPE-g-MAH) prepared under different conditions was studied. The grafting reaction conditions are presented in Table 2. In this case, two different MAH and initiator concentrations were employed. The presence of succinic anhydride grafts onto ethylene sequences of ULDPE can alter its natural capability to crystallize depending on the grafting site.

We have previously reported that the chemical modification of polyethylene does not significantly alter its melting and crystallization behavior, when the grafting degree of the materials is not high enough [38]. Figure 9 shows DSC heating scans of neat and functionalized ULDPE. No appreciable differences between modified and pure material can be seen. In general, a slight depression in the melting peak temperature (T_m) with increasing grafting degree can be observed. This suggests that a reduction of the mean lamellar thickness of the samples is promoted by the introduction of anhydride groups. However, these results do not allow a relationship between reaction conditions and the obtained products to be established. In fact, a lowering of about 9°C in T_m was observed for ULDPE-G16 and ULDPE-G12 as compared to neat ULDPE (Tables 1 and 2) but these two samples have different grafting degrees and therefore no conclusions could be drawn from this fact.

As can be seen in Table 2, both groups, ULDPE-G4 and ULDPE-G8, and ULDPE-G12 and ULDPE-G16, have the same initiator concentration but different MAH concentration. It is reasonable that ULDPE-G8 and ULDPE-G16 had higher grafting degrees compared to their respective pairs; with a higher MAH concentration, there is an increase in the probability that MAH molecules link to PE macroradicals. At the same time, these grafts could interrupt ethylene sequences, in-

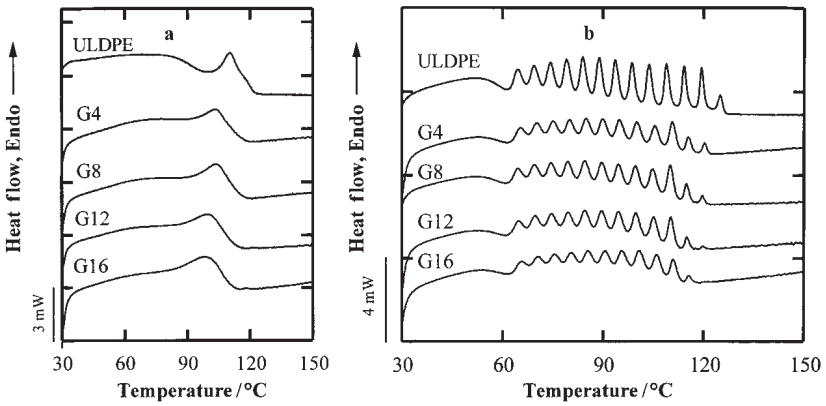

Fig. 9 DSC heating scans at 10°C min^{-1} for neat ULDPE and ULDPE-g-MAH: a – after a controlled cooling at 10°C min^{-1}, and b – after SSA thermal treatment

troducing imperfections into the chain, which will lead to lower lamellar thickness. Traditional heating DSC scans (Fig. 9) or cooling scans (not shown here), did not confirm this assumption, because roughly the same T_m was observed in each case.

When SSA technique was used for the analysis of the above materials (also Fig. 9), a higher decrease in the peak area corresponding to thicker crystals (high T_m) for ULDPE-G8 was seen, as compared to ULDPE-G4, and for ULDPE-G16 as compared to ULDPE-G12. An interruption in the linear sequences of ULDPE chains could explain this behavior.

On the other hand, if we observed those materials with the same MAH concentration but different initiator concentration (groups ULDPE-G4 and G12, and ULDPE-G8 and G16), at higher initiator levels, both, higher grafting degrees and lower T_m were observed in each case. With an increasing initiator concentration, there are more free radicals to promote reaction between molecules, but at the same time, a higher concentration of initiator can favor collateral reactions like free macroradicals combination instead of MAH grafting [37]. This fact can result in lowering the grafting degree, and at the same time, interruption of linear sequences that could be able to crystallize at lower undercoolings. As it was expected from previous analysis, a reduction in peak area corresponding to linear sequences was observed for ULDPE-G12 with respect to ULDPE-G4 and for ULDPE-G16 with respect to ULDPE-G8.

It is clear from the above discussion and from a general comparison in Fig. 9 of ULDPE with any of its functionalized versions, that the SSA can immediately reveal the depletion of the most linear fractions within the ULDPE. This fact as mentioned in specific cases above, is indicating that grafting reactions are occurring preferentially in the secondary carbons within the main chain, even though the MAH grafting onto tertiary carbons is not ruled out. In this case, the SSA was very helpful to confirm a reaction mechanism that was very difficult to postulate just on the basis of FTIR and 1H NMR results [30]. These results confirm similar findings with LLDPE and LLDPE grafted with diethyl maleate [4].

Application of SSA to characterize LDPE and XLDPE

Figure 10 shows heating DSC scans of neat LDPE and after crosslinking (i.e., XLDPE). A comparison is made between untreated samples and samples that were submitted to an SSA treatment. Table 1 indicates that a reduction of 4°C in T_m was observed for the XLDPE in comparison to the LDPE and a reduction in crystallinity degree was also detected. These are the expected changes since crosslinking induced by peroxide initiator causes a random radical reaction that will involve proton abstraction from secondary carbons in the chains for later recombination reactions. Therefore, the linear portions of the chains originally available for crystallization will be shortened randomly.

The final heating scan after SSA for LDPE is shown in Fig. 10. The distribution of melting points after fractionation is unimodal in contrast with that of LLDPE. This is a result of the distribution of chain branches in LDPE. Chain branches in LDPE are normally long since they originate in chain transfer reactions that occur during radical polimerization at high pressures. Here again, the radical chain transfer reactions oc-

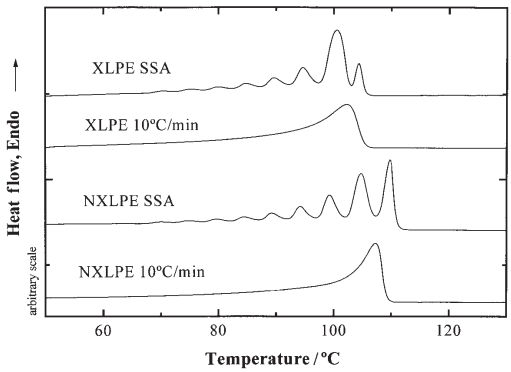

Fig. 10 DSC heating scans at 10°C min^{-1} for LDPE and XLDPE: after a controlled cooling at 10°C min^{-1}, and after SSA thermal treatment (as indicated on the curves)

cur in random fashion without preferred specific sites of the growing chain, therefore, a unimodal distribution of chain branches is generated.

If the heating scan after SSA of the XLDPE is considered, a new distribution of melting points, lamellar thickness and chain branches can be observed as compared to the unmodified LDPE. The fraction with the highest melting point in LDPE (i.e., T_m=109.7°C) corresponds to the fusion of the thicker lamellae conformed by the most linear chains in the polymer. In the XLDPE this fraction has been completely depleted by the crosslink reactions. Furthermore, the fraction with the second highest melting point (i.e., T_m=104.7°C) in LDPE is present in a lower amount in the XLDPE, where the most abundant fraction is the one that melts at around 99°C. A quantitative analysis of the areas under each peak can give a quantitative idea of the changes induced by the cross-linking reaction [1, 5].

The SSA technique can give valuable insight into the thermal history of an insulator that coats a high voltage conducting wire. If the SSA is performed on an unused XLDPE insulator, a curve relating T_m *vs.* T_s can be obtained similar to that in Fig. 6. After an ordinary DSC scan is performed on a XLDPE sample that has already a thermal history (e.g., after simulated aging in the laboratory, using high voltages during specific time cycles or after real service), the scan will reflect the previous history of the sample exhibiting complex melting endotherms that can be made up of several peaks [39]. The exact origin of each peak can be trace back to specific annealings at different T_s temperatures during aging or service life using the SSA derived T_m *vs.* T_s curve. Then simulated SSA programs can determine the annealing times requires for each melting peak to develop a specific height and enthalpy of fusion. In this way, the SSA may be useful to characterize wire coating failures during service life [39].

Application of SSA to characterize a LLDPE block within ABC triblock copolymers

In a previous work, polystyrene-block-poly(ethylene-co-butylene)-block-poly(ε-caprolactone) triblock copolymers (SEC) were prepared by hydrogenating polystyrene-block-polybutadiene-block-poly(ε-caprolactone) triblock copolymers (SBC) previ-

ously prepared by sequential anionic polymerization [29]. The effect of the crystallization of the polyethylene block (PE) upon cooling from a phase segregated melt on the crystallization process of the adjacent polycaprolactone block (PCL) was investigated by means of DSC and polarized optical microscopy [3, 29]. It was found that there was no nucleation effect of the PE block on the PCL block under controlled cooling conditions in the DSC. On the contrary, an antinucleation effect was detected when nucleation of the PCL block crystals within the SEC triblock copolymers was attempted. It was demonstrated that such antinucleation effect was induced by the annealing of the polyethylene block crystals with the smallest lamellar sizes of the SEC copolymers [3].

Applying SSA to these copolymers the possibility of producing a distribution of lamellar thickness within the PCL and the PE blocks of the SEC triblock copolymers can be explored [3]. The polyethylene center block is equivalent in structure to a LLDPE since it contains butyl branches (9–11 mass%) but its chain ends are confined by the other two blocks. Under these confined circumstances it could be difficult to produce a distribution of lamellar thickness within this semicrystalline block. In a previous work [3], we hinted that producing a distribution of lamellar thickness within one microphase constituted by one of the blocks was possible in spite of the chain constrains, but the SSA treatment applied used heating rates of 20°C min^{-1} which were not optimum to show the details of the fractionation that can be induced by SSA. Figure 11 instead shows that using 10°C min^{-1} in all the SSA steps including the final heating run leaves no doubt that the center block can still be self-nucleated and annealed. If a comparison with LLDPE is made (Fig. 5) it is noticeable that the separation between fractions is not as clear (i.e., the resolution is not as good, peaks are broad and not as well defined as in the LLDPE case) for the LLDPE restricted block case in view of its more difficult chain diffusion characteristics.

The influence of copolymer composition in the SSA results of Fig. 11 is very interesting. The copolymer that can form the largest amount of thicker lamellae is $S_{27}E_{37}C_{36}$ since this is the copolymer with the highest amount of PE in its structure. Therefore, the

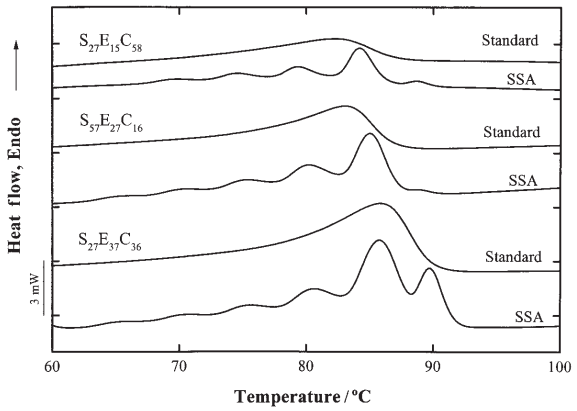

Fig. 11 DSC heating scans at 10°C min^{-1} for $S_{27}E_{37}C_{36}{}^{132}$, $S_{27}E_{15}C_{58}{}^{219}$, $S_{57}E_{27}C_{16}{}^{137}$, after a controlled cooling at 10°C min^{-1} (labelled 'Standard'), and after SSA thermal treatment (as indicated on the curves)

PE chains in the center block will be less constrain to diffuse and produce thicker lamellae during the annealing process than $S_{27}E_{15}C_{58}$ where at least the proportion of PS is similar. The reason behind the almost absence of the highest melting point fraction in the $S_{57}E_{27}C_{16}$ copolymer is related to the high content of PS in this copolymer (PS is already in the glassy state when the PE component crystallizes). In the case of the unhydrogenated analogue of this material, $S_{57}B_{27}C_{16}$, morphological observations have shown that the PS phase constitutes the matrix where core shell polygonal microdomains of PCL and PB are embedded with the PB forming the outer shell in between the PCL and the PS micro-phase. This means that the PB is completely surrounded by vitrified PS limiting the mobility of this phase. In other words, the behavior is most probably dominated also in the SEC case by the morphology which is at the moment under study.

We have also applied SSA to other multiphase polymeric materials and have demonstrated the usefulness of the technique for studying the miscibility of polyolefin blends [5].

Conclusions

The successive self-nucleation and annealing (SSA) technique is a powerful tool that can be used to characterize any semicrystalline polymer that undergoes molecular segregation when cooled from the melt and therefore can be thermally fractionated. It is particularly well suited for polymers that contain a certain amount of chain branches or random comonomer sequences that can interrupt the linear portions of crystallizable chains. It does not require special instrumentation and can be performed with almost any DSC. SSA is simpler and quicker than TREF but the fractions obtained can not be physically separated from one another.

* * *

This work was made possible by the financial support of the 'Consejo Venezolano de Investigaciones Científicas y Tecnológicas' (CONICIT) through Grant G97-000594 and that of the 'Decanato de Investigación y Desarrollo' from Simón Bolívar University through Grant DID-G02. We would like to acknowledge the contribution of Y. Paolini, who did the DSC experiments on the LDPE and XLDPE samples. Valuable discussions with J. L. Feijoo, J. Ramírez and E. Da Silva are also acknowledged with thanks.

References

1 A. J. Müller, Z. H. Hernández, M. L. Arnal and J. J. Sánchez, Polym. Bull., 39 (1997) 465.
2 M. L. Arnal, Z. H. Hernández, M. Matos, J. J. Sánchez, G. Mendez, A. Sánchez and A. J. Müller, Proc. of the ANTEC 1998, SPE 56 (1998) 2007.
3 V. Balsamo, A. J. Müller and R. Stadler, Macromolecules, 31 (1998) 7756.
4 L. Márquez, I. Rivero and A. J. Müller, Macromol. Chem. Phys., 200 (1999) 330.
5 M. L. Arnal, J. J. Sánchez and A. J. Müller, Proc. of the ANTEC 1999, SPE 57 (1999) 2329.
6 R. Popli and L. Mandelkern, J. Polym. Sci. Polym. Phys. Ed., 25 (1987) 441.
7 V. B. F. Mathot and M. F. J. Pijpers, J. Appl. Polym. Sci., 39 (1990) 979.

8 M. A. Kennedy, A. J. Peacock, M. D. Failla, J. C. Lucas and L. Mandelkern, Macromolecules, 28 (1995) 1407.
9 C. Bruni, M. Pracella, F. Masi, F. Menconi and F. Ciardelli, Polym. Intern., 33 (1994) 279.
10 P. Starck, Polym. Intern., 40 (1996) 111.
11 L. Wild, T. R. Ryle, D. C. Knobeloch and I. R. Peat, J. Polym. Sci. Polym. Phys. Ed., 20 (1982) 441.
12 V. B. F. Mathot and M. F. J. Pijpers, Polym. Bull., 11 (1984) 297.
13 P. L. Joskowicz, A. Muñoz, J. Barrera and A. J. Müller, Macromol. Chem. Phys., 196 (1995) 385.
14 P. Schouterden, G. Groeninckx, B. Van der Heijden and F. Jansen, Polymer, 28 (1987) 2099.
15 T. Kamiya, N. Ishikawa, S. Kambe, N. Ikegami, H. Nishibu and T. Hattori, Proc. of the ANTEC 1990, SPE, (1990) 871.
16 E. Adisson, M. Ribeiro, A. Deffieux and M. Fontanille, Polymer, 33 (1992) 4337.
17 T. M. Liu and I. R. Harrison, Thermochim. Acta, 233 (1994) 167.
18 M. Y. Keating and E. F. McCord, Thermochim. Acta, 243 (1994) 129.
19 J. J. Mara and K. P. Menard, Acta Polymerica, 45 (1994) 378.
20 G. Balbotin, I. Camurati, T. Dall'Occo, A. Finotti, R. Franzese and G. Vecellio, Die Angewandte Makromolekulare Chemie, 219 (1994) 139.
21 F.-C. Chiu, M. Y. Keating and S. Z. D. Cheng, Proc. of the ANTEC 1995, SPE 53 (1993) 1503.
22 M. Zhang, J. Huang, D. T. Lynch and S. Wanke, Proc. of the ANTEC 1998, SPE 56 (1998) 2000.
23 R. A. Shanks and K. Drummond, Proc. of the ANTEC 1998, SPE 56 (1998) 2004.
24 B. Fillon, J. C. Wittman, B. Lotz and A. Thierry, J. Polym. Sci. B, 31 (1993) 1383.
25 O. O. Santana and A. J. Müller, Polym. Bull., 32 (1994) 471.
26 R. A. Morales, M. L. Arnal and A. J. Müller, Polym. Bull., 35 (1995) 379.
27 A. C. Manaure, R. A. Morales, J. J. Sánchez and A. J. Müller, J. Appl. Polym. Sci., 66 (1997) 2481.
28 M. L. Arnal, M. E. Matos, R. A. Morales, O. O. Santana and A. J. Müller, Macromol. Chem. Phys., 199 (1998) 2275.
29 V. Balsamo, A. J. Müller, F. von Gyldenfeldt and R. Stadler, Macromol. Chem. Phys., 199 (1998) 1063.
30 A. Sánchez, C. Rosales and A. J. Müller, to be published.
31 R. H. Olley, A. M. Hodge and D. C. Basset, J. Polym. Sci. Phys. Ed., 17 (1979) 627.
32 E. Cañizales, C. Urbina, M. L. Arnal and A. J. Müller, to be published.
33 U. W. Gedde, Polymer Physics, Chapman & Hall, London, (1995).
34 L. Lu, R. G. Alamo and L. Mandelkern, Macromolecules, 27 (1994) 6571.
35 Ch. Han and H.-K. Chuang, J. Polym. Sci., 30 (1985) 2431.
36 E. G. Koulouri, K. G. Gravalos and J. K. Kallitsis, Polymer, 37 (1996) 2555.
37 N. C. Liu, W. E. Baker and K. E. Russell, J. Appl. Polym. Sci., 41 (1990) 2285.
38 A. Sánchez, C. Rosales and A. J. Müller, Proc. of the ANTEC 1997, SPE 55 (1997) 3761.
39 Y. Paolini, G. Ronca, J. L. Feijoo, E. Da Silva, J. Ramírez and A. J. Müller, to be submitted (1999).